Cellular and Molecular Life Sciences (2023) 80:364
https://doi.org/10.1007/s00018-023-05011-3

ORIGINAL ARTICLE

SARS-CoV-2 ORF6 protein targets TRIM25 for proteasomal degradation to diminish K63-linked RIG-I ubiquitination and type-I interferon induction

Oyahida Khatun[1,2] · Mansi Sharma[1,2] · Rohan Narayan[1,2] · Shashank Tripathi[1,2]

Received: 8 July 2023 / Revised: 6 October 2023 / Accepted: 23 October 2023 / Published online: 20 November 2023

Abstract

Evasion and antagonism of host cellular immunity upon SARS-CoV-2 infection provide replication advantage to the virus and contribute to COVID-19 pathogenesis. We explored the ability of different SARS-CoV-2 proteins to antagonize the host's innate immune system and found that the ORF6 protein mitigated type-I Interferon (IFN) induction and downstream IFN signaling. Our findings also corroborated previous reports that ORF6 blocks the nuclear import of IRF3 and STAT1 to inhibit IFN induction and signaling. Here we show that ORF6 directly interacts with RIG-I and blocks downstream type-I IFN induction and signaling by reducing the levels of K63-linked ubiquitinated RIG-I. This involves ORF6-mediated targeting of E3 ligase TRIM25 for proteasomal degradation, which was also observed during SARS-CoV-2 infection. The type-I IFN antagonistic activity of ORF6 was mapped to its C-terminal cytoplasmic tail, specifically to amino acid residues 52–61. Overall, we provide new insights into how SARS-CoV-2 inhibits type-I IFN induction and signaling through distinct actions of the viral ORF6 protein.

Keywords SARS-CoV-2 · Type-I IFN · ORF6 · RIG-I · TRIM25 · Ubiquitination

Introduction

While the COVID-19 pandemic wanes in its third year, its etiological agent SARS-CoV-2 stays at the focus of the intense scientific investigation by researchers across the globe. Tremendous progress has been made on the front of vaccine and antiviral development against COVID-19; however, the fundamental biology of the virus is still being explored. SARS-CoV-2 is a single-stranded positive-sense RNA virus of the family *Coronaviridae* that also includes at least four known seasonal coronaviruses and more pathogenic SARS and MERS coronaviruses [1]. The genome comprises two overlapping open reading frames (ORFs), ORF1a and ORF1b, which are translated to generate continuous polypeptides and subsequently cleaved into 16 non-structural proteins (NSPs) [2]. One shared aspect of *Betacoronaviruses* is their ability to evade and antagonize the host's innate and adaptive immune responses [3]. This property is essential for efficient virus infection and replication and contributes to viral pathogenesis. Especially in the case of COVID-19, the dampening of early cellular innate immune response and subsequent dysregulation of cytokine expression is considered a significant contributor to severe disease. Hence, a detailed investigation into viral mechanisms of host immune evasion and antagonism is essential for developing effective therapeutic interventions.

One of the earliest cellular antiviral responses is orchestrated by IFNs, which pose a crucial hurdle that viruses must overcome upon infection. IFN response begins with recognition of viral pathogen-associated molecular patterns (PAMPs) by cellular Pattern Recognition Receptors (PRRs). In lung epithelial cells, MDA5 acts as the primary sensor of SARS-CoV-2 RNA and governs the innate immune response [4, 5]. RIG-I is also reported as a sensor and triggers type-I IFN expression [4, 6]. These PRRs relay the message through specific kinases to transcription factors IRF3, IRF7, and NF-kB, which in turn induce expression of type-I, II, or

✉ Shashank Tripathi
shashankt@iisc.ac.in

1 Emerging Viral Pathogens Laboratory, Centre for Infectious Disease Research, Indian Institute of Science, Bengaluru, India

2 Microbiology and Cell Biology Department, Biological Sciences Division, Indian Institute of Science, Bengaluru, India

III IFNs [7, 8]. Subsequently, IFNs activate the JAK-STAT pathway in an autocrine or paracrine manner, leading to the expression of a battery of interferon-stimulated genes (ISGs) that act as viral restriction factors and regulators of innate and adaptive immunity [9]. Viruses have evolved a plethora of mechanisms to inhibit IFN induction and subsequent signaling events to counteract host innate immunity [10], and SARS-CoV-2 is no exception [11, 12]. SARS-CoV-2 has a 29.7 kb single-stranded positive-sense RNA genome. About two-thirds of the 5′ end of the genome encodes ORF1a/1b, which in turn produces 16 NSPs after proteolytic processing of polyprotein 1a and 1ab (pp1a and pp1ab); about 10 kb of genome at the 3′ end encodes multiple sub-genomic RNAs that get translated into 4 structural proteins [Spike (S); Envelope (E); Membrane (M); and Nucleocapsid (N)] and at least 9 accessory proteins (ORF3a; 3b; 6; 7a; 7b; 8; 9b; 9c and 10) [13, 14]. Many SARS-CoV-2 accessory and NSPs have been reported to have antagonistic effects on IFN responses [3].

In this study, we screened the IFN-antagonistic ability of SARS-CoV-2 proteins and found ORF6, among others, to be the most potent inhibitor of both IFN induction and signaling. We mapped these activities to the cytoplasmic tail of ORF6, specifically the residues 52–61, which are highly conserved. Our data were consistent with earlier studies where ORF6 was shown to inhibit IFN response by blocking the nuclear import of key transcription factors involved in IFN response. However, these events are downstream in the IFN induction pathway, and the molecular basis of the highly efficient shutdown of IFN induction by SARS-CoV-2 ORF6 protein was unclear. Here, for the first time, we show that ORF6 directly interacts with RIG-I and inhibits early stages of type-I IFN induction. RIG-I activation requires K63-linked ubiquitination by E3 ligase TRIM25 [15]. We observed that the presence of SARS-CoV-2 ORF6 protein leads to reduced levels of K63-linked RIG-I and proteasomal degradation of TRIM25. The reduction of TRIM25 protein level and rescue upon proteasomal inhibition was also observed in SARS-CoV-2 infected cells. Overall, our data provide new insights into the molecular mechanisms of IFN antagonism mediated by the SARS-CoV-2. Specifically, we show that in addition to inhibition of nuclear translocation of IRF3 and STAT1, which are late events of IFN response, SARS-CoV-2 ORF6 protein inhibits early steps of this pathway at the level of RIG-I activation.

Materials and methods

Plasmids

Plasmids expressing SARS-CoV-2 proteins were a kind gift from Prof. Nevan Krogan (University of California San Francisco) and have been described before [16]. The IFN induction and signaling plasmids (IFNβ-Firefly Luciferase, ISRE-Firefly Luciferase, pRL-TK, RIG-I, 2-CARD, TBK1, IKKe, IRF3-5D, IRF7-CA, STAT1, STAT2) were provided by Prof. Adolfo García-Sastre (Icahn School of Medicine at Mount Sinai, New York) and have been described before [17]. For constructing the deletion mutants, the desired sequence was PCR amplified from pLVX-EF1alpha-SARS-CoV-2-ORF6-2xStrep-IRES-Puro plasmid, followed by cloning in the pCAGGS backbone using EcoRI (ER0271, Thermo Scientific) and XhoI (ER0691, Thermo scientific) restriction enzyme including the full-length ORF6. ΔC plasmid was constructed using overlap extension PCR. ORF6 variant mutants were constructed by subcloning the construct in a TA backbone, followed by substituting the residues as described before [18] and cloning in the pCAGGS backbone using EcoRI and XhoI. We procured pRK5-HA-Ubiquitin-K63 (RRID: Addgene_17606) and pRK5-HA-Ubiquitin-K48 (RRID:Addgene_17605) from Addgene.

Cell lines and cell culture

Human embryonic kidney 293 T (HEK293T, RRID:CVCL_0063), A549 lung adenocarcinoma, and HeLa cells (RRID:CVCL_0030) were purchased from the National Centre for Cell Science (NCCS, Pune), and HEK-ACE2 (RRID: CVCL_A7UK), Vero E6 cells (RRID:CRL-1586) were procured from the America Type Culture Collection (ATCC, Bethesda, MD). Cells were cultured in complete media containing high-glucose Dulbecco's modified Eagle's medium (DMEM) (12100–046, Gibco) with 10% FBS (16140–071, Gibco), penicillin–streptomycin (Gibco 15140–122), supplemented with GlutaMAX™ (35050–061, Gibco) at 37 °C with 5% CO_2.

Viruses and infection

SARS-CoV-2 (Isolate Hong Kong/VM20001061/2020, BEI Resources Cat# NR-52282, NIAID, NIH) was propagated and titered by plaque assay in Vero E6 cells as described before [19]. HEK-ACE2 (for SARS-CoV-2) or HEK293T (for Sendai Virus) were seeded in a 24-well cell culture dish (pre-coated with 0.1 mg/mL poly-L-lysine (P9155-5MG, Sigma-Aldrich)) and 24 h later, used for infection. Infection was done with 1 MOI SARS-CoV-2 in DMEM supplemented with 10% FBS or 100 HAU SeV in OPTI-MEM in 100 µl inoculum for 1 h with intermittent shaking every 10 min at 37 °C. Fresh complete DMEM was added to the cells.

Plasmid transfection

HEK-293 T cells (0.1 X 10^6 cells/well) were seeded in a 24-well plate pre-coated with 0.1 mg/mL poly-L-lysine

(P9155-5MG, Sigma-Aldrich) and 24 h later used for transfection. Cells were then transfected with 0.5 µg of expression plasmid using Lipofectamine-2000 reagent (Invitrogen Cat#11668019) or Lipofectamine-3000 (Invitrogen Cat# L3000015), according to the manufacturer's instruction.

Luciferase reporter assay

For the IFN induction assay, HEK-293 T cells (0.1 X 10^6 cells/well in a 24-well plate) were co-transfected, in duplicates, with 50 ng of pIFNβ -luc and 20 ng of pRL-TK along with 500 ng of SARS-CoV-2 protein expression plasmid or empty vector. 24 h post-transfection, cells were induced with poly (I:C) (1 µg), or 100 HAU of Sendai virus for 12 h, followed by lysing of the cells for analyzing the dual luciferase activity. For dissecting the steps of the IFN induction pathway, HEK-293 T cells were co-transfected with 50 ng of inducer plasmid along with the above-indicated plasmids. 24 h post-transfection, cells were lysed. Similarly, for the IFN signaling assay, HEK-293 T cells (0.1 X 10^6 cells/well in a 24-well plate) were co-transfected with 50 ng of ISRE-luc Firefly Luciferase reporter plasmid and 20 ng of pRL-TK Renilla Luciferase reporter plasmid along with 500 ng of SARS-CoV-2 protein expression plasmid. 24 h post-transfection, the cells were induced with 1000 U/ml of Universal Type-I IFN (PBL assay, Cat # 11200–1). 12 h post-induction, the cells were lysed, and luciferase activity was measured using a dual-luciferase assay system (Promega Cat# E1980) according to the manufacturer's instructions. Firefly and Renilla Luciferase signals were quantified using Tecan plate reader (INFINITE M PLEX). The signals were represented as percentage fold change with respect to the induced vector.

Immunofluorescence assay (IFA) and quantification

A549 cells were seeded on coverslips in a 24-well plate (0.1 X 10^6 cells per well) for overnight incubation. They were then co-transfected with 500 ng of IRF3-GFP and 500 ng of SARS-CoV-2 protein-expressing plasmid using Lipofectamine-2000 reagent (Invitrogen Cat# 11668019). 24 h post-transfection, the cells were induced with 6 h of Sendai virus infection (100 HAU). Similarly, Vero cells were seeded on coverslips in 24-well plates (0.1 X 10^6 cells/well) for overnight incubation. Cells were then transfected with 250 ng of STAT1-GFP along with 250 ng of SARS-CoV-2 viral protein-expressing plasmids. 24 h post-transfection, cells were induced for 1 h with 1000 U/ml Universal Type-I interferon (IFN) (PBL Assay Science Cat# 11200–2). Similarly, HeLa cells were transfected with 250 ng of RIG-I Flag or MAVS Flag and 250 ng of ORF6 strep for 24 h. A549-ACE2 cells were seeded on coverslips in a 24-well plate (0.1 X 106 cells per well), and 24 h later, cells were infected with SARS-CoV-2 at 1 MOI. 6 h post-infection cells were treated with MG132 (10 µM) for another 18 h. Cells were washed with 1X PBS (MP Biomedicals Cat# 162528) twice at room temperature and fixed in PBS with 4% formaldehyde (Qualigen Cat# Q24005) at room temperature for 20 min. The cells were then permeabilized using 1% Tween-20 (Sigma-Aldrich Cat# P1379) in PBS at room temperature for 10 min. After three washes with 1X PBS, cells were incubated in blocking buffer, 2% BSA (MP Biomedicals Cat# 0215240105) in 1X PBS containing 0.3% Tween-20, at room temperature (RT) for 2 h, followed by washing twice with wash buffer (PBS with 0.3% Tween 20). Coverslips were incubated with primary antibody at a 1:500 ratio diluted in 50 µl PBS with 0.3% Tween 20 and 0.5% BSA for 3 h at RT. Used primary antibodies are rabbit anti-Strep-tag II antibody (abcam cat# ab76949, RRID:AB_1524455), mouse monoclonal ANTI-FLAG® (Sigma-Aldrich Cat# F3165-0.2MG, RRID:AB_259529), SARS-CoV / SARS-CoV-2 (COVID-19) spike antibody (GeneTex Cat# GTX632604, RRID:AB_2864418), Recombinant Anti-TRIM25/EFP antibody [EPR7315] (abcam Cat# ab167154, RRID:AB_2721902). Cells were washed thrice with wash buffer followed by incubation with secondary antibody (1:1000) for 2 h at RT in the dark using following antibodies: Goat anti-Mouse IgG (H + L) Cross-Adsorbed Secondary Antibody, Alexa Fluor 488 (Invitrogen cat# A-11001, RRID:AB_2534069), Donkey anti-Rabbit IgG (H + L) Highly Cross-Adsorbed Secondary Antibody, Alexa Fluor™ 568 (Invitrogen Cat# A10042, RRID:AB_2534017), Goat anti-Rabbit IgG (H + L) Cross-Adsorbed Secondary Antibody, Alexa Fluor™ 488 (Thermo Cat# A11008, RRID:AB_143165), Goat anti-Mouse IgG (H + L) Cross-Adsorbed Secondary Antibody, Alexa Fluor™ 568 (Thermo Cat# A11004, RRID:AB_2534072). The cells were washed thrice with wash buffer and counter-stained with 4',6-diamidino-2-phenylindole (DAPI), (Sigma-Aldrich Cat# D9542-10MG) for 10 min at RT. Coverslips were washed thrice with PBS and mounted on a slide using antifade mounting media (Invitrogen Cat# P36970) and imaged using Zeiss 880 or Leica SP8 confocal microscope. For quantification of IRF3-GFP nuclear translocation, line region of interests were drawn across the nucleus and fluorescence intensity of GFP (green) and DAPI (blue) channels were quantified along the length using Imagej/Fiji. The values were used to calculate the area under the curve of green signal overlapping with blue. The fluorescence intensity of TRIM25 labeled cells was quantified using Leica LASX microscope software. The fluorescence intensity of RIG-I Flag labeled cells was quantified by using Imagej/Fiji.

Co-immunoprecipitation (Co-IP) and immunoblotting

Transfected cells were washed with ice-cold 1X PBS and then were lysed using 500 μl Pierce lysis buffer supplemented with phosphatase and protease inhibitor, per 100 mm dish. The lysate was incubated on ice for 30 min with vigorous vortexing every 10 min. Samples were sonicated (25% amplitude, 5-s ON-5-s OFF for two cycles) and clarified by centrifugation at 13,000 rpm for 10 min at 4 °C. The clarified supernatant was either stored at −80 °C or analyzed by immunoblotting as whole cell lysate (WCL or Input). Lysates were pre-cleared with magnetic beads coated with protein-G, and immunoprecipitation was performed for the remaining lysates by overnight incubation with specific antibodies. Subsequently, the complex was pulled down by magnetic beads coated with protein-G (88847, Invitrogen) according to the manufacturer's instructions. Elution was done directly by 1X Laemmli buffer (BIO-RAD Cat#1610747). Protein samples were resolved by SDS–polyacrylamide gel electrophoresis, followed by transfer onto a PVDF membrane (Immobilon-P; Merck Cat# IPVH00010). Blocking was performed at room temperature for 2 h using 5% skimmed milk (HiMedia Cat# GRM1254-500G) in 1X PBS containing 0.05% Tween 20 (Sigma-Aldrich Cat# P1379) (1X PBST). Afterward, primary antibody incubation was performed overnight (12 h) at 4 °C with slow rocking using primary antibodies: Rabbit anti-Strep-tag II antibody (abcam cat# ab76949), Mouse monoclonal ANTI-FLAG® M2 antibody (Sigma-Aldrich Cat# F3165-0.2MG, RRID:AB_259529), rabbit DYKDDDDK Tag (D6W5B) Rabbit mAb (Binds to the same epitope as Sigma's Anti-FLAG® M2 Antibody) (Cell Signaling Technologies cat# 14793S, RRID:AB_2572291), Beta-Actin Monoclonal Antibody (BA3R), HRP (Thermofisher Scientific Cat# MA5-15739-HRP, RRID:AB_2537667), Biotin Anti-HA tag antibody (abcam Cat# ab26228, RRID:AB_449023), V5-Tag (D3H8Q) Rabbit mAb (Cell Signaling Technologies Cat# 13202, RRID:AB_2687461), TRIM25 Monoclonal Antibody (5B5B12) (Thermofisher Cat# MA5-31935, RRID:AB_2787558), Recombinant Anti-TRIM25/EFP antibody [EPR7315] (abcam Cat# ab167154, RRID:AB_2721902), SARS-CoV/SARS-CoV-2 (COVID-19) spike antibody (GeneTex Cat# GTX632604, RRID:AB_2864418), SARS-CoV/SARS-CoV-2 Nucleocapsid Antibody, Rabbit Mab (Sino Biologicals Cat# 40143-R004, RRID Number: AB_2827975). Secondary antibody incubation was performed at room temperature for 2 h using corresponding secondary antibody: Goat Anti-Mouse IgG H&L (Thermofisher Cat# 31430, RRID:AB_228307), Goat Anti-Rabbit IgG H&L (Thermofisher Cat# 31460, RRID:AB_228341). The proteins were visualized using Clarity Western ECL Substrate (BIO-RAD Cat# 1705061).

Quantitative real-time PCR

1 µg of RNA was reverse transcribed into cDNA using Prime Script™ RT Reagent Kit with gDNA Eraser (Perfect Real Time) (Takara-Bio Cat# RR047A) and then diluted fivefold with nuclease-free water (MP Biomedicals Cat# 112450204). The gene expression study was conducted using PowerUp™ SYBR™ Green Master Mix (Applied Biosystems™ Cat# A25778) with 18S rRNA as the internal control and appropriate primers for the genes.

Graphical representations and statistical analysis

All numerical data of luciferase assays and qRT-PCR were analyzed and plotted using GraphPad Prism v8.0.2. Statistical significance was calculated using a *t* test with Bonferroni corrections for multiple comparisons (wherever necessary). The P values were indicated as $*P < 0.05$; $**P < 0.01$; $***P < 0.001$; ns = not significant. Error bars represent mean + standard error. The model diagram of ORF6 action (Fig. 8) and 3D structure (Fig. 3A) were made using Biorender.

Results

Multiple SARS-CoV-2 proteins antagonize type-I IFN induction and signaling

We began the study intending to identify all the SARS-CoV-2 proteins that may interfere with type-I IFN induction. For this, we co-transfected plasmids expressing SARS-CoV-2 proteins in HEK-293 T cells with an interferon-beta (IFNβ) promoter-driven Firefly Luciferase reporter plasmid (pIFNβ-FFLuc) and a control plasmid constitutively expressing Renilla Luciferase gene (pRL-TK). After 24 h, we treated the cells with poly (I:C) to stimulate the type-I IFN induction pathway, and relative luciferase units were measured 12 h post-stimulation. We observed that NSP1, NSP5, NSP6, NSP7, NSP10, NSP13, NSP14, NSP15, and ORF6 reduced IFN reporter induction to less than 30% of control. We kept the cutoff 30% to keep maximum coherence with published datasets related to IFN antagonism by SARS-CoV-2 proteins (Fig. 1A). Similarly, to identify the SARS-CoV-2 proteins, which may interfere with type-I IFN signaling and ISG induction, we co-transfected SARS-CoV-2 plasmids with an ISRE promoter-driven Firefly Luciferase reporter plasmid (pISRE-FFLuc), along with pRL-TK. Cells were treated with universal interferon to stimulate type-I IFN signaling and ISG induction. Relative Luciferase Units (RLUs) were calculated, and as before, we observed that NSP1, NSP5, NSP13, NSP14, and ORF6 reduced ISG induction

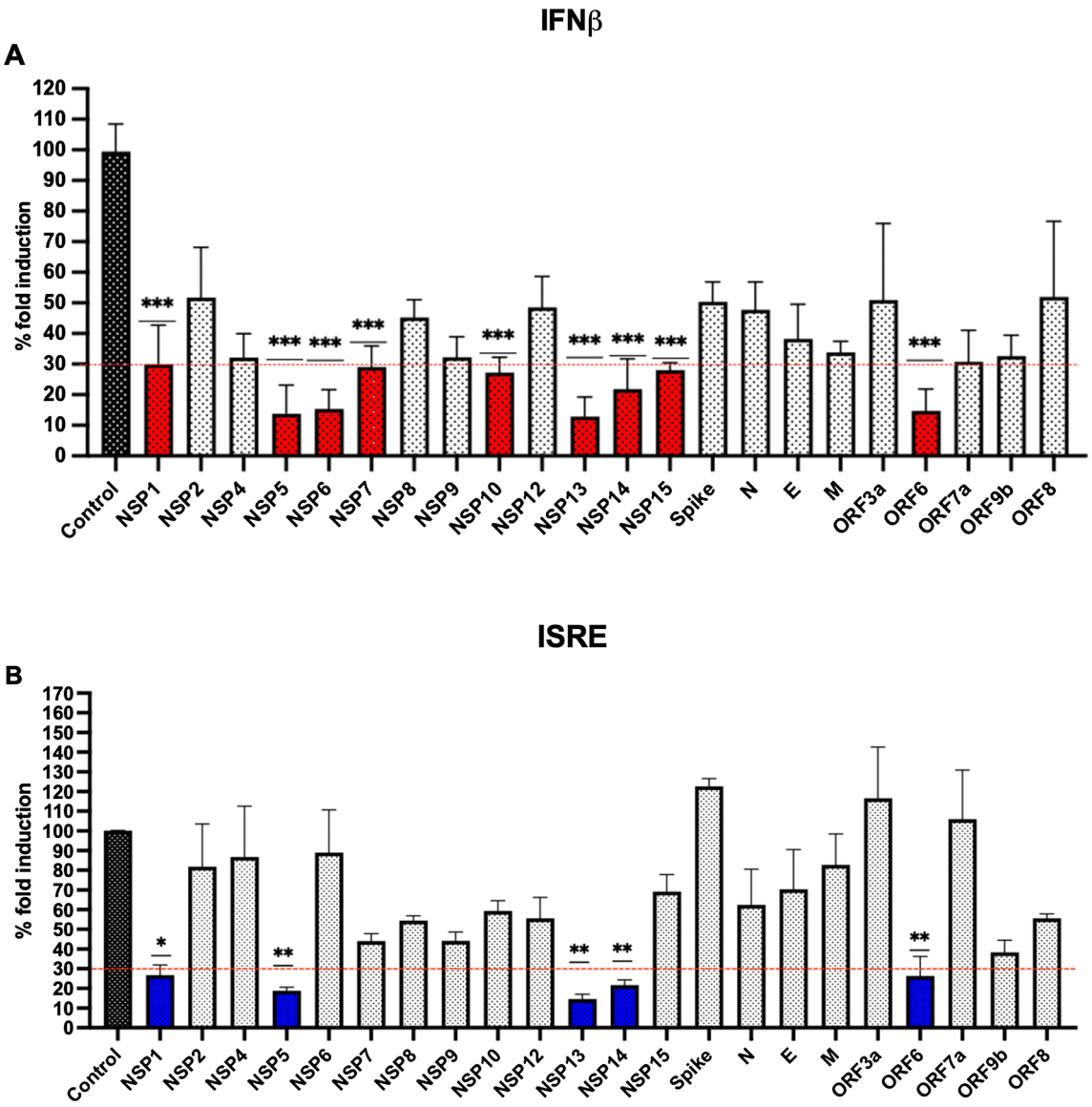

Fig. 1 Multiple SARS-CoV-2 proteins antagonize type-I IFN induction and signaling. **A** Quantification of IFNβ dual luciferase assay of all SARS-CoV-2 proteins. HEK293T cells were co-transfected with IFNβ promoter-driven Firefly Luciferase reporter plasmid, Renilla Luciferase reporter plasmid, and viral protein-expressing plasmid or empty vector. 24 h post-transfection, cells were induced with poly I:C, followed by assaying the cells for dual luciferase activity. **B** Quantification of ISRE dual luciferase assay of SARS-CoV-2 proteins. HEK293T cells were co-transfected with ISRE promoter-driven Firefly Luciferase reporter plasmid, Renilla Luciferase reporter plasmid, and viral protein-expressing plasmid or empty vector. 24 h post-transfection cells were induced with Universal Type I IFN (1000U/ml) for 12 h, followed by which cells were assayed for dual luciferase activity. Bar graphs represent data from three biological repeats, with four technical replicates. Statistical significance of the data is represented as $*P<0.05$; $**P<0.01$; $***P<0.001$; *ns* not significant. Error bars represent mean + standard error

to less than 30% of control (Fig. 1B). We ensured that these effects on IFN induction and signaling were consistent with SARS-CoV-2 protein expression by validating their expression (Supplementary Fig. 1A). While all constructs were expressed at variable levels, the NSP11, ORF3b, and ORF7b constructs did not produce a detectable band by western blot (Supplementary Fig. 1A). Apart from the earlier mentioned proteins, a few additional proteins also inhibited IFN induction (NSP4, NSP8, NSP9, NSP12, N, E, M, ORF7a, ORF9b) or signaling (NSP7, NSP9, ORF9b), though less effectively (Supplementary Fig. 1B). During screening all the proteins, NSP3 was not included as the plasmid was present in a different expression vector. However, it is reported that NSP13 inhibits ISG15-dependent activation of MDA5 by de-ISGylation [20]. Also, it cleaves IRF3 using its proteolytic activity

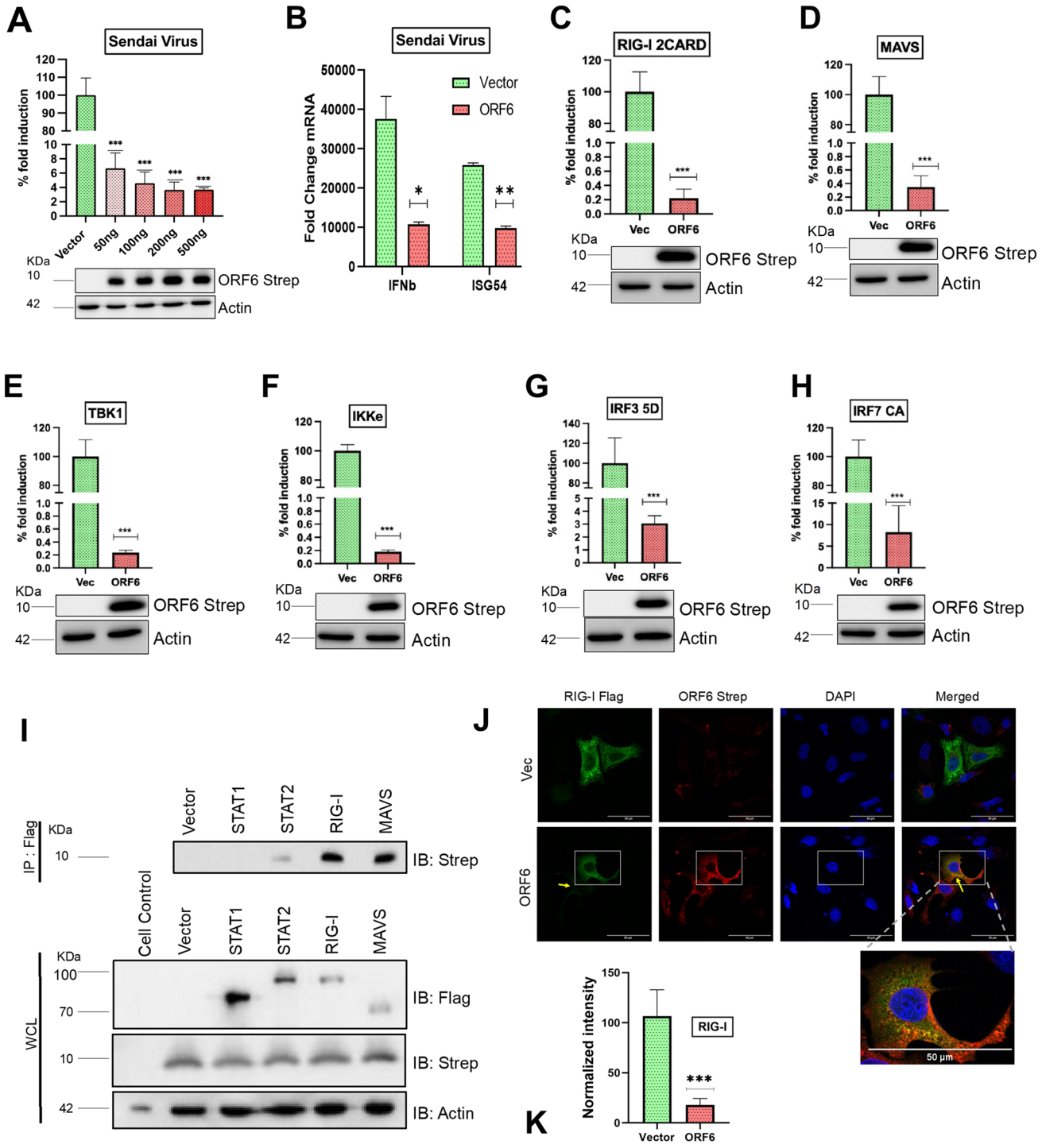

[21]. To further substantiate our results, we compiled and compared the data from previous studies where similar reporter-based approaches were utilized to screen for IFN antagonists of SARS-CoV-2 (Supplementary Fig. 1C, D) [11, 12, 22–28]. Our findings largely corroborated other studies, and this comparison revealed ORF6 as the most consistent and effective inhibitor of IFN induction and signaling across various studies (Supplementary Fig. 1C, D) [11, 12, 23, 24, 26–29]. Hence, we decided to further explore the mechanistic aspects of type-I IFN antagonism by SARS-CoV-2 ORF6 protein.

◂**Fig. 2** SARS-CoV-2 ORF6 protein inhibits type-I IFN induction and signaling through distinct mechanisms. **A** Effects of increasing amounts of ORF6 on IFNβ promoter activation. HEK293T cells were co-transfected with IFNβ promoter-driven Firefly Luciferase reporter plasmid, Renilla Luciferase reporter plasmid, and increasing amounts of ORF6 expressing plasmid or empty vector. 24 h post-transfection cells were infected with Sendai virus for 12 h, followed by assaying the cells for dual luciferase activity. **B** mRNA levels of IFNβ induction pathway protein (IFNβ) and signaling pathway protein (ISG54) were measured from total RNA from HEK293T cells transfected with ORF6 or empty vector followed by Sendai virus infection. **C–H** Effect of of SARS-CoV-2 ORF6 on IFNβ promoter activation in presence of different IFN induction pathway inducer protein. HEK293T cells were co-transfected with Firefly Luciferase reporter plasmid driven by IFNβ promoter, Renilla Luciferase reporter, plasmid expressing ORF6 or empty vector, and as an inducer, plasmid expressing RIG-I 2CARD (**C**), MAVS (**D**), TBK1 (**E**), IKKε (**F**), IRF3-5D (**G**) or IRF7-CA (**H**). 24 h post-transfection, cells were lysed for dual luciferase activity analysis. **i** Co-immunoprecipitation of ORF6-strep and innate immune pathway proteins. HEK293T cells were co-transfected with ORF6-strep and STAT1-, STAT2-, RIG-I-, and MAVS-Flag. Whole cell lysates (WCL) were incubated with anti-Flag antibody followed by analyzing the eluate by western blot. **J** Representative confocal images showing the co-localization of RIG-I (green) and ORF6 (red). HeLa cells were co-transfected with RIG-I Flag and ORF6-strep or empty vector for 24 h followed by immunostaining. Scale bar 50 µm. Here the left yellow arrow shows a reduction in expression in RIG-I expression, and the right yellow arrow shows co-localization of RIG-I and ORF6. Bar graphs represent data from three biological repeats, with four technical replicates. Statistical significance of the data is represented as $*P<0.05$; $**P<0.01$; $***P<0.001$; *ns* not significant. Error bars represent mean + standard error

SARS-CoV-2 ORF6 protein inhibits type-I IFN induction and downstream signaling through distinct mechanisms

Next, we tested the IFN-antagonistic ability of ORF6 in the context of virus infection. We observed that SARS-CoV-2 ORF6 could inhibit IFNβ-Luciferase induction in Sendai virus (SeV) infected cells, in a dose-dependent manner (Fig. 2A). This was corroborated by measuring the effect of ORF6 expression on IFNβ and ISG54 transcript levels by RT-PCR in SeV-infected cells (Fig. 2B). To further confirm the IFN-antagonistic activity of SARS-CoV-2 ORF6 protein, we performed dose–response experiments and found that it can inhibit IFNβ and ISRE promoter-driven Luciferase expression in a dose-dependent manner (Supplementary Fig. 2A, B). To identify the specific targets of ORF6, we performed an IFNβ Luciferase assay in the presence of different signaling components leading to type-I IFN induction. We observed that ORF6 inhibited IFNβ induced by RIG-I 2CARD, MAVS, TBK1, IKKe, IRF3-5D (a constitutively active form of IRF3), and IRF7-CA (a constitutively active form of IRF7) to varying degrees, with the very prominent effect seen at the level of RIG-I (Fig. 2C–H). This was confirmed in an experiment where ORF6 inhibited RIG-I 2CARD-induced IFNβ reporter activity in a dose-dependent manner (Supplementary Fig. 2C). To further investigate this, we examined the interaction of ORF6 with key mediators of IFN induction and signaling, including RIG-I, MAVS, STAT1, and STAT2, and found that ORF6 interacted with all of them except STAT1 (Fig. 2I). Immunofluorescence assays further confirmed this, which showed significant ORF6 co-localization with RIG-I (Fig. 2J) and to a limited extent with MAVS (Supplementary Fig. 2D). We also showed that ORF6 expression reduces the RIG-I intensity in IFA (Fig. 2K). Earlier studies have reported that ORF6 interferes with the nuclear translocation of transcription factors involved in IFN induction (IRF3) and signaling (STAT1). This was corroborated in our experiments where ORF6 expression inhibited SeV infection-induced nuclear translocation of IRF3 and STAT1 (Supplementary Fig. 3A, B). Overall, these data indicated that ORF6 inhibits both type-I IFN induction and downstream signaling leading to ISG induction by targeting different components of these pathways.

The cytoplasmic domain of SARS-CoV-2 ORF6 is essential for type-I IFN antagonism

SARS-CoV-2 ORF6 protein is a 61 amino acid accessory protein [27]. Its ortholog is present in SARS-CoV but absent in the MERS virus [30]. The C-terminus of the SARS-CoV ORF6 is critical for innate immune antagonism [31]. This prompted us to map the domains and amino acid residue of SARS-CoV-2 ORF6, essential for type-I IFN response antagonism. Structural homology modeling predicted the ORF6 protein to comprised N (M1-Q8)-terminal and C (N47-D61)-terminal cytoplasmic tails and a middle transmembrane domain (V9-E46) (Fig. 3A) [32]. SARS-CoV-2 ORF6 shares a 69% sequence similarity with its SARS-CoV counterpart [27]. Sequence alignment of SARS-CoV-2 with other closely related coronaviruses showed that N-terminus cytoplasmic part (M1-Q8) and C-terminus cytoplasmic part (N47-D61) residues are relatively conserved (Supplementary Fig. 4A). To understand the evolutionary changes in different domains of ORF6, we aligned the consensus sequence of SARS-CoV-2 variants of concern (VOCs) (Supplementary Fig. 4B). Results showed the protein to be entirely conserved, except in the cytoplasmic tail of Omicron VOC. Furthermore, we compared the IFN antagonistic activity of ORF6 proteins from SARS-CoV and SARS-CoV-2 and found the latter to be slightly more potent (Supplementary Fig. 4C, D). To map the IFN antagonistic activity of ORF6 to its distinct domains, we created expression constructs lacking the N-terminus (ΔN), and C-terminus (ΔC) (Fig. 3B). Next, we tested the ability of ORF6-specific domain deletion constructs to inhibit IFN and ISG induction using the luciferase reporter assay. We observed that

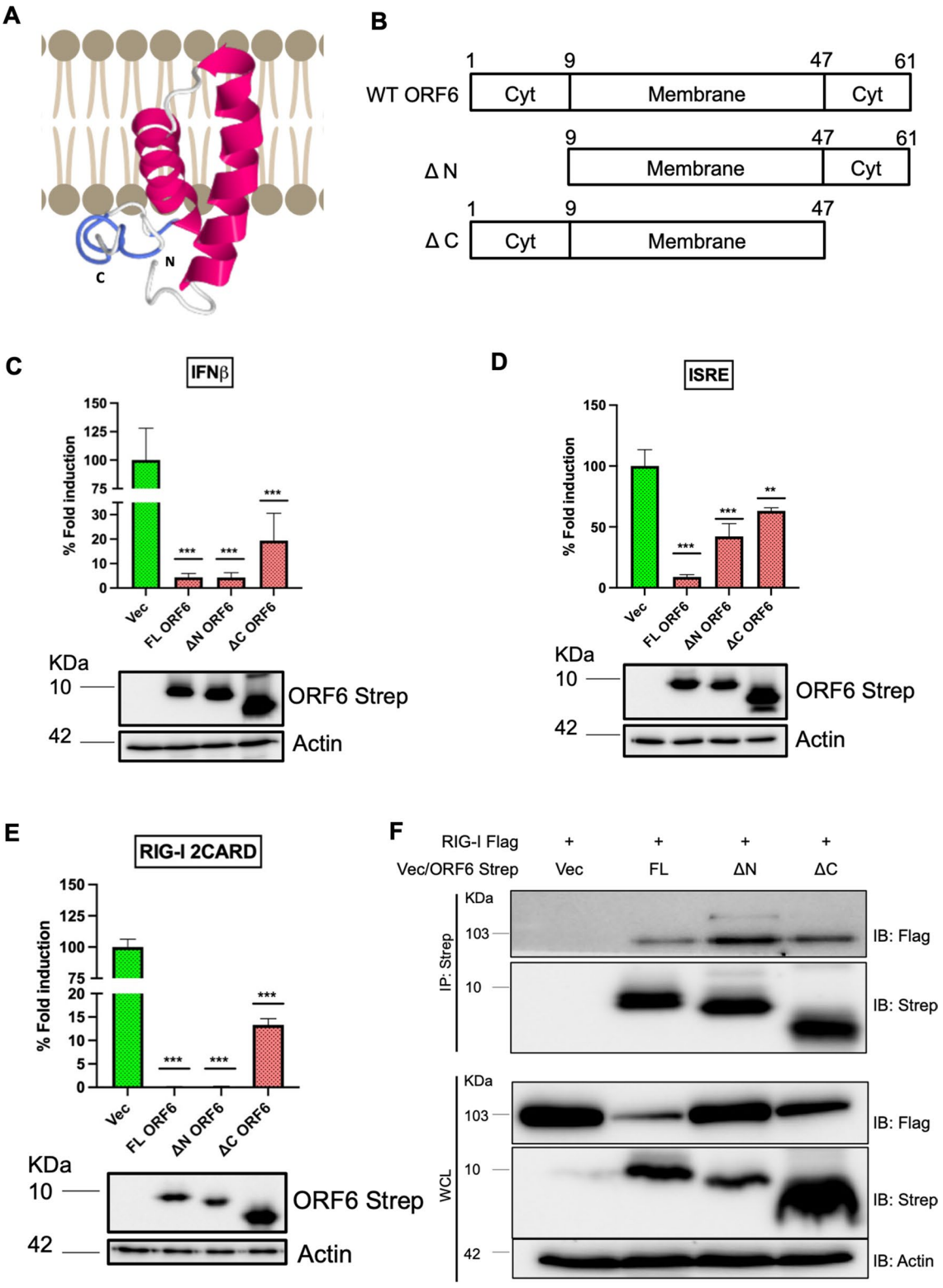
A
C
N
B
WT ORF6
1
9
47
61
Cyt
Membrane
Cyt
Δ N
Membrane
Cyt
Δ C
Cyt
Membrane
C
IFNβ
% Fold induction
150
125
100
75
30
20
10
0
***
Vec
FL ORF6
ΔN ORF6
ΔC ORF6
KDa
10
42
ORF6 Strep
Actin
D
ISRE
% Fold induction
150
100
50
0
***
**
Vec
FL ORF6
ΔN ORF6
ΔC ORF6
KDa
10
42
ORF6 Strep
Actin
E
RIG-I 2CARD
% Fold induction
150
125
100
75
20
15
10
5
0
***
Vec
FL ORF6
ΔN ORF6
ΔC ORF6
KDa
10
42
ORF6 Strep
Actin
F
RIG-I Flag + + + +
Vec/ORF6 Strep Vec FL ΔN ΔC
KDa
103
10
IP: Strep
IB: Flag
IB: Strep
KDa
103
10
42
WCL
IB: Flag
IB: Strep
IB: Actin

◂**Fig. 3** The cytoplasmic domain of SARS-CoV-2 ORF6 is essential for type-I- IFN antagonism. **A** Three-dimensional predicted model structure of ORF6. Prediction was done using I-TASSER (Iterative Threading Assembly Refinement) standalone software version 5, which was visualized using Jmol 14.32. The final image was made using Biorender.com. **B** Schematic representation of the domain structure of ORF6 and involved amino acids. It consists of two cytoplasmic domains in N- and C-terminus and a membrane domain in the middle. Here wild type is WT, ΔN is where the N-terminal cytoplasmic domain is deleted, and ΔC where the C-terminal domain is deleted. **C**, **D** Dual-luciferase assay depicting the effect of full length (FL) and deletions of ORF6 on IFNβ (**C**) and ISRE (**D**) promoter activation. HEK293T cells were co-transfected with IFNβ promoter-driven Firefly Luciferase reporter plasmid (**E**), or ISG-promoter-driven Firefly Luciferase reporter plasmid (**D**), Renilla Luciferase reporter plasmid, and ORF6 variants expressing plasmid or empty vector. 24 h post-transfection, cells were induced with poly I:C (**C**) or Universal Type I IFN (1000 U/ml) (**D**) for 12 h, followed by assaying the cells for dual luciferase activity. **E** Dual luciferase assay showing the effect of FL and deletions of ORF6 on IFNβ promoter activation in presence of RIG-I 2CARD. HEK293T cells were co-transfected with Firefly Luciferase reporter plasmid driven by IFNβ promoter, Renilla Luciferase reporter, plasmid expressing ORF6 or empty vector, and as an inducer, plasmid expressing RIG-I 2CARD. 24 h post-transfection, cells were lysed for dual luciferase activity analysis. **F** Co-immunoprecipitation (Co-IP) of RIG-I Flag and ORF6-strep FL and deletions. HEK 293 T cells were co-transfected with RIG-I Flag and empty vector or different deletions of ORF6-strep. 48 h post-transfection, cells were lysed, and whole cell lysates (WCL) were incubated overnight with anti-strep antibody followed by adding magnetic beads. Eluates and WCL were analyzed by western blot with indicated antibodies. Bar graphs represent data from three biological repeats, with four technical replicates. Statistical significance of the data is represented as $*P<0.05$; $**P<0.01$; $***P<0.001$; *ns* not significant. Error bars represent mean + standard error

ΔC constructs significantly lost the ability to inhibit IFN induction and downstream signaling (Fig. 3C, D). In comparison, ΔN was still effective in inhibiting IFN induction but less in restricting ISRE activity than full-length (FL) ORF6 (Fig. 3D). The importance of the C-terminal domain in inhibiting IFN induction was further validated using RIG-I 2CARD as inducer. Here also ΔC construct was significantly less effective than full-length ORF6 in inhibiting IFNβ induction (Fig. 3E). We also tested the effect of ORF6-specific domain deletions on RIG-I interaction by co-immunoprecipitation and IRF3 nuclear translocation by immunofluorescence. Although we did not see the loss of interaction with RIG-I with ORF6 upon domain deletion, there was an overall reduced expression of RIG-I in the presence of ORF6, which was significantly rescued in both N and C domain deletions (Fig. 3F). Furthermore, while the full length and ΔN ORF6 were still effective in restricting IRF3 to the cytoplasm in SeV-infected cells, ΔC ORF6 lost this ability to do the same (Supplementary Fig. 5A, B). Concomitantly, we also observed that ΔC constructs rescued the IFNβ promoter activation in presence of IRF3-5D expressing plasmid as inducer (Supplementary Fig. 5C). Overall, these data established that the C-terminal cytoplasmic domain of the SARS-CoV-2 ORF6 protein is crucial for its ability to restrict both type-I IFN induction and downstream ISG induction.

Amino acid residues 52–61 in the C-terminal tail of ORF6 are crucial for its IFN antagonistic function

The SARS-CoV-2 ORF6 protein has a conserved amino acid stretch from 52 to 61 aa in the C-terminal tail, implicated in IFN antagonism (Fig. 4A) [11]. To validate that, we constructed four amino acid long alanine scanning mutations with two amino acid overlaps, called ORF6 M1 (aa 52–55), M2 (aa 54–57), and M3 (aa 56–59) and M4 (58–61) (Fig. 4A). We tested the expression of these constructs by western blotting, where ORF6 M1 and M2 migrated slightly lower compared to the wild-type protein, indicating possible sites of post-translational modification between residues 52 and 57 (Fig. 4B). Next, we tested the ability of these ORF6 mutants to inhibit IFNβ induction due to RIG-I 2CARD and IRF3-5D. Here we observed that all the mutants from M1 to M3 progressively lost their IFN antagonism against both RIG-I and IRF3, with ORF6 M3 and M4 showing maximum loss (Fig. 4B, C). Interestingly, all ORF6 mutants were equally ineffective in mitigating ISRE-driven luciferase expression (Fig. 4D). These data suggest that although the C-terminal tail of ORF6, especially residues 52–61 of ORF6, is crucial for antagonizing IFN induction and signaling, and they play distinct roles in antagonizing different components of these signaling processes.

The cytoplasmic tail of SARS-CoV-2 ORF6 reduces K63-linked ubiquitinated RIG-I levels

So far, we had observed that SARS-CoV-2 ORF6 protein could very potently inhibit RIG-I mediated type-I IFN induction, and its C-terminus tail was crucial for this activity. However, the deletion of the cytoplasmic tail had no obvious impact on the direct interaction between RIG-I and ORF6. Hence, we speculated that perhaps ORF6 interferes with RIG-I at the post-transcriptional or post-translational level. We observed that ORF6 reduced RIG-I mRNA level by 50% (Fig. 5A), which is significant but does not explain the complete inhibition of RIG-I-mediated IFNβ induction. The inhibitory effect of ORF6 on total RIG-I protein level was not reversed by proteasomal inhibition through MG132 treatment in the presence of K63-linked ubiquitination (Fig. 5B). RIG-I is known to undergo post-translational modification in the form of ubiquitination, which can regulate its activity and stability depending on the nature of the linkage [33]. To understand the impact of ORF6 on this aspect, we examined wild-type, K48- and K63-linked ubiquitination of RIG-I in the presence or absence of ORF6

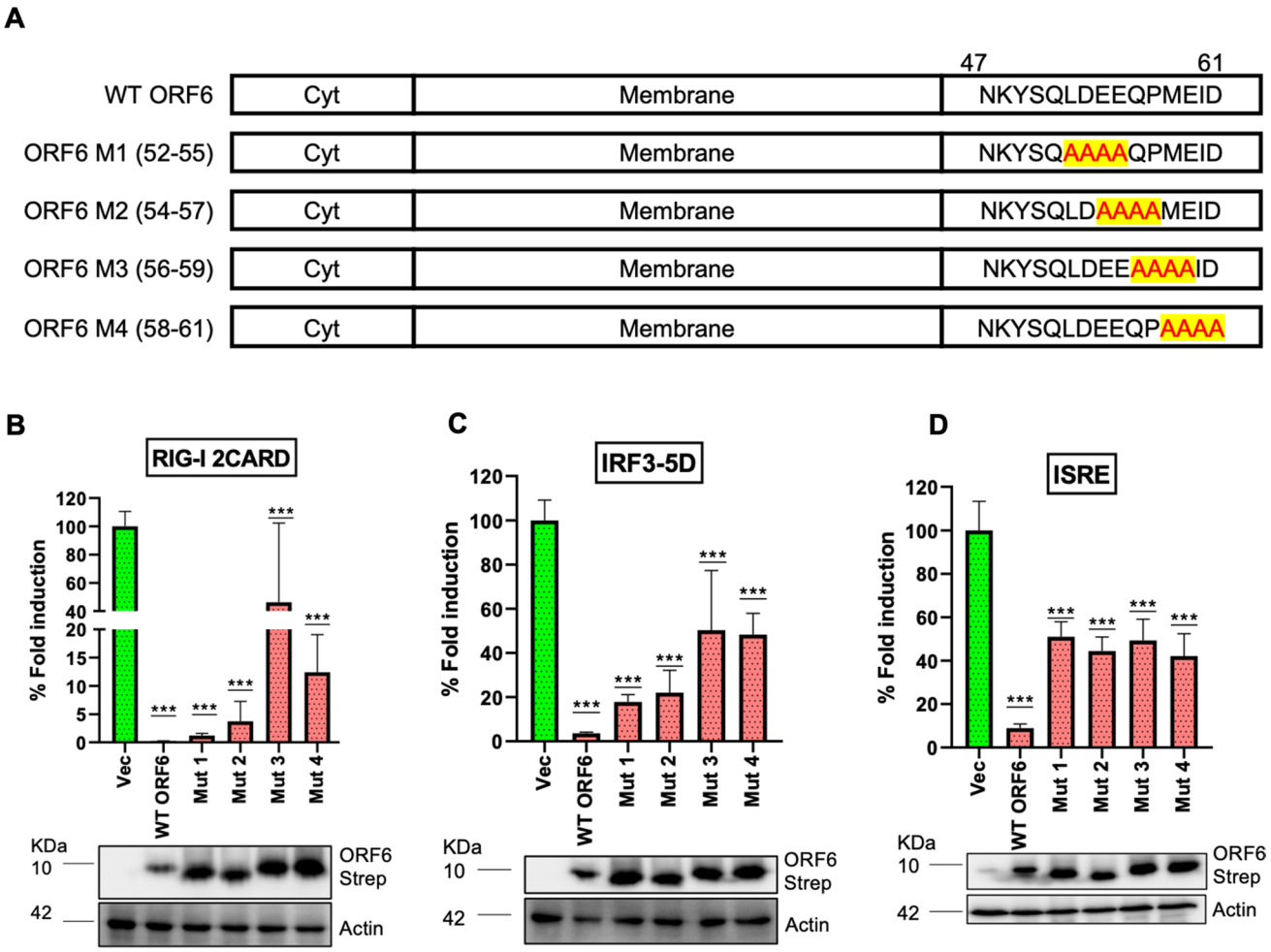

Fig. 4 Amino acid residues 52–61 in the C-terminal tail of ORF6 are crucial for its IFN antagonistic function. **A** Schematic diagram of ORF6 variants. Four amino acids are converted to alanine by site-directed mutagenesis (highlighted in yellow color) for different variants construction. Here, WT: wild type, M1: mutant 1, amino acids 52–55 are substituted with alanine, M2: mutant 2, 54–57 amino acids are substituted with alanine, M3: mutant 3, 56–59 amino acids are converted to alanine, and M4: mutant 4, 58–61 amino acids are converted to alanine. **B**, **C** Effect of ORF6 variants on IFNβ promoter activation upon RIG-I-2CARD (**B**) and IRF3-5D (**C**) induction. HEK293T cells were co-transfected with Firefly Luciferase reporter plasmid driven by IFNβ promoter, Renilla Luciferase reporter, plasmid expressing ORF6 WT or mutants or empty vector, and as an inducer, plasmid expressing RIG-I 2CARD (**B**), or IRF3-5D (**C**). 24 h post-transfection, cells were lysed for dual luciferase activity analysis. **D** Dual luciferase assay depicting the effect of ORF6 variants on ISRE promoter activation. HEK293T cells were co-transfected with ISG-promoter-driven Firefly Luciferase reporter plasmid**,** Renilla Luciferase reporter plasmid, and WT or ORF6 mutants expressing plasmid or empty vector. 24 h post-transfection, cells were induced with Universal Type I IFN (1000U/ml) for 12 h, followed by assaying the cells for dual luciferase activity. Bar graphs represent data from three biological repeats, with four technical replicates. Statistical significance of the data is represented as $*P<0.05$; $**P<0.01$; $***P<0.001$; *ns* not significant. Error bars represent mean + standard error

in an immunoprecipitation experiment. We observed that the presence of ORF6 reduced all forms of ubiquitination of RIG-I, with the most prominent effect seen on K63-linked RIG-I (Supplementary Fig. 6A, B). Further, we performed an IP experiment to test the ability of SARS-CoV-2 ORF6-specific domain deletion constructs to interfere with K63-linked RIG-I ubiquitination. We observed that both full-length and ΔN ORF6 were effective; however, ΔC ORF6 lost its ability to reduce K63-linked ubiquitinated RIG-I levels (Fig. 5C, D). Overall, these data suggested that ORF6 reduced K63-linked ubiquitinated RIG-I, which is its active form responsible for type-I IFN induction.

SARS-CoV-2 ORF6 targets TRIM25 for proteasomal degradation to inhibit K63-linked ubiquitination of RIG-I

The K63-linked ubiquitination of RIG-I is mediated by E3 ligase TRIM25 [15]. Thus, we explored the effect of ORF6 on mRNA level and protein levels of TRIM25 and

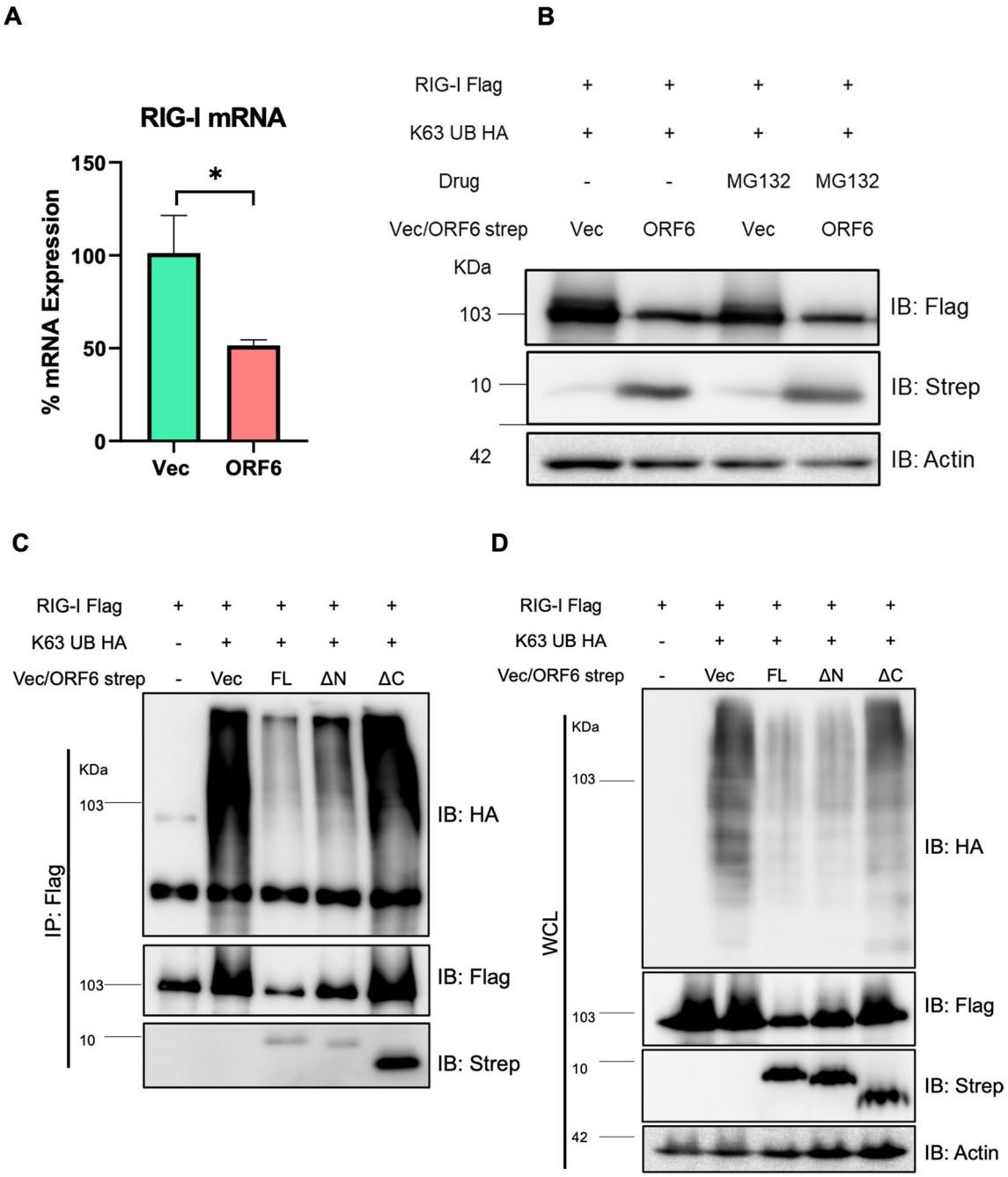

Fig. 5 Cytoplasmic tail of SARS-CoV-2 ORF6 reduces K63-linked ubiquitinated RIG-I levels. **A** RIG-I mRNA levels were measured from total RNA from HEK293T cells co-transfected with RIG-I and ORF6 or empty vector for 36 h. **B** Western blot analysis with cell lysates from HEK 293 T cells co-transfected with RIG-I Flag, K63-linked ubiquitin HA, and strep-tagged ORF6 or empty vector 24 h followed by MG132 (10 μM) treatment for 12 h. **C**, **D** Western blot analysis with cell lysates from HEK293T cells co-transfected with RIG-I Flag, K63-linked UB HA, and different deletions of ORF6-strep or empty vector. Cell lysates were either directly assessed as WCL (**D**) or incubated overnight with anti-Flag antibody followed by analysis as IP fraction (**C**) and probed with indicated antibodies

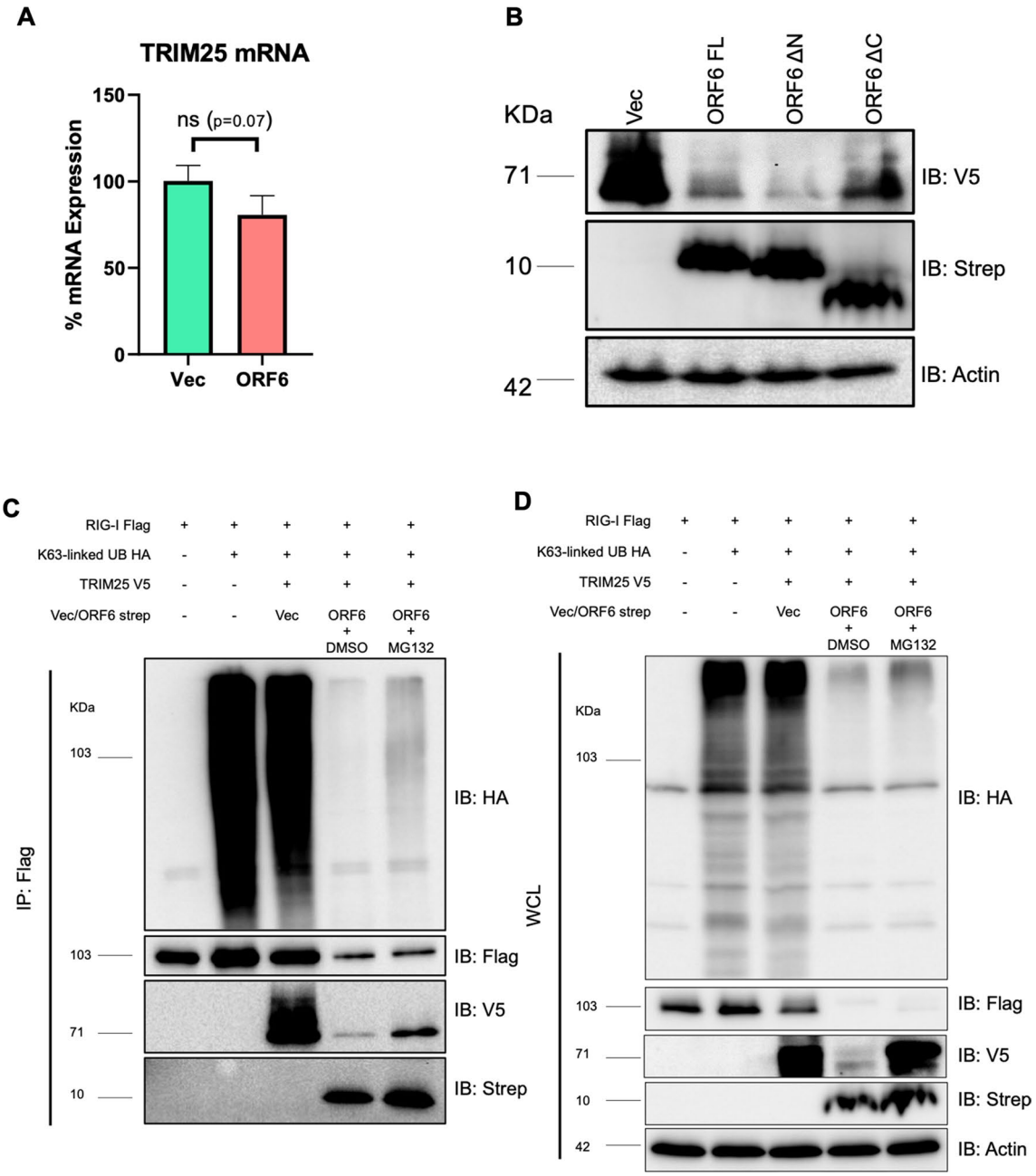

Fig. 6 SARS-CoV-2 ORF6 targets TRIM25 for proteasomal degradation to inhibit K63-linked ubiquitination of RIG-I. **A** TRIM25 mRNA levels were measured from total RNA from HEK293T cells co-transfected with TRIM25 and ORF6 or empty vector for 36 h. **B** Western blot analysis with cell lysates from HEK 293 T cells co-transfected with TRIM25 V5 and empty vector or strep-tagged ORF6 (FL or ΔN or ΔC for 48 h. **C**, **D** Western blot analysis with cell lysates from HEK293T cells co-transfected with RIG-I Flag, K63-linked UB HA, TRIM25 V5 and empty vector or ORF6-strep for 24 h, followed by MG132 treatment (10 μM) for 12 h. Cell lysates were either directly assessed as WCL (**D**) or incubated overnight with anti-Flag antibody followed by analysis as IP fraction (**C**) and probed with indicated antibodies

concomitant K63-linked ubiquitination of RIG-I in the presence of TRIM25. We found a very marginal reduction in TRIM25 mRNA in presence of ORF6 (Fig. 6A). However, we observed a very strong reduction in TRIM25 protein level in presence of FL and ΔN ORF6, which was rescued in the presence of ΔC ORF6 (Fig. 6B). Viruses often co-opt cellular proteasome machinery to target innate immune signaling mediators for degradation [34, 35]. Thus, we examined the effect of ORF6 on the TRIM25 protein levels and K63-linked ubiquitination of RIG-I, and the effect of proteasomal inhibition by MG132 on the same. We observed that ORF6 expression drastically reduced protein levels of both RIG-I and TRIM25 upon overexpression of K63-linked ubiquitin; however, only TRIM25 was selectively rescued upon MG132 treatment (Fig. 6C, D). We also performed IP experiments to assess the effect of ORF6 on the levels of TRIM25-mediated K63-linked ubiquitination of RIG-I. We observed in the IP fraction of the MG132-treated cells, there was partial rescue of K63-linked RIG-I (Fig. 6C) which is coherent with TRIM25 rescue in total cell lysate (Fig. 6D). These data indicated that ORF6 targets TRIM25 for proteasomal degradation, which leads to reduced K63-linked ubiquitination of RIG-I.

SARS-CoV-2 targets TRIM25 for proteasomal degradation during infection to mitigate IFN induction

Next, we examined the effect of SARS-CoV-2 infection on TRIM25 degradation. The proteasomal degradation of TRIM25 was also observed in the case of SARS-CoV-2 infected HEK-ACE2 cells and was rescued by MG132 treatment (Fig. 7A). This was concomitant with reduced expression of viral Spike protein, indicating a negative effect of MG132 treatment and TRIM25 rescue on viral replication (Fig. 7A). Although this phenotype was weaker (Fig. 7B) as compared to ORF6 overexpression experiments, normalization of TRIM25 with viral protein expression showed significant rescue of TRIM25 in infected cells upon MG132 treatment (Fig. 7C). Moreover, we also observed that MG132 treatment enhanced the expression of IFNβ mRNA and downstream ISGs such as ISG54 and TRIM25 itself (Supplementary Fig. 7A–C). Furthermore, we validated our observation of TRIM25 depletion during SARS-CoV-2 infection and rescue of the same by MG132 treatment in A549-ACE2 cells. In western blotting analysis, differences in the protein levels were not reflected clearly, possibly due to larger uninfected cell background (Fig. 7D). To address this, we performed IFA and quantified the intensity of TRIM25 and Spike expression in the infected cells (Fig. 7E). Quantification of protein signals showed clear increase in TRIM25 and decrease in Spike levels upon MG132 treatment (Fig. 7F). Taken together, these data confirm the phenomenon of proteasomal degradation of TRIM25 during SARS-COV-2 infection.

Discussion

SARS-CoV-2 encodes at least 27 proteins categorized into structural, non-structural, and accessory proteins. While structural proteins, such as Spike are direct targets of humoral immunity and are under constant selection pressure, the accessory and non-structural proteins are often engaged in antagonism and evasion of cellular innate immunity, primarily driven by interferon. The IFN antagonism by SARS-CoV-2 has been a subject of intense research by several groups, and significant progress has been made in understanding it. In particular, the type-I IFN, which is produced by all respiratory tract epithelial cells to combat viral infection, is targeted by multiple SARS-CoV-2 accessory and non-structural proteins in multiple ways, often with overlapping mechanisms [11, 12, 22–29, 36]. This study started with experimentally cataloging the SARS-CoV-2 proteins that either inhibit type-I IFN induction or the downstream signaling to produce ISGs or inhibit both. We observed that four SARS-CoV-2 proteins (NSP1, NSP13, NSP14, and ORF6) were able to potently inhibit both type-I IFN induction and signaling, which was in coherence with multiple independent studies. The NSP1 protein has been shown to directly interact with ribosomes and cause cellular mRNA translation shutdown. This also results in the inhibition of the production of IFNs and ISGs during viral infection [37]. The NSP14 protein has been reported to shut down host translation, whereas NSP13 hijacks deubiquitinase USP13 to restrict IFN induction [38, 39]. In our experiments, the ORF6 protein was effective in inhibiting both type-I IFN induction and downstream signaling. Several other research groups have also reported such activity of SARS-CoV-2 ORF6, and the mechanism behind this has been mapped to the inhibition of nuclear import of transcription factors (STAT1, IRF3) crucial for IFN response. It does so by associating with the nuclear import co-factor Karyopherin alpha and nuclear pore-component Nup98 [12, 31, 40]. These interactions also allow ORF6 to restrict the nuclear export of cellular RNAs induced upon infection, which may also contribute to its IFN antagonistic activity [41].

In our study, SARS-CoV-2 ORF6 was found to exert a strong inhibitory action on RIG-I-mediated type-I IFN induction, which is a very early step of RLR signaling upstream of nuclear translocation of IRF3 or expression of ISGs. Direct action of ORF6 on RIG-I was not reported or examined before; hence, we decided to explore this in more detail. We found that ORF6 directly interacts and co-localizes with RIG-I and leads to its reduced expression. The

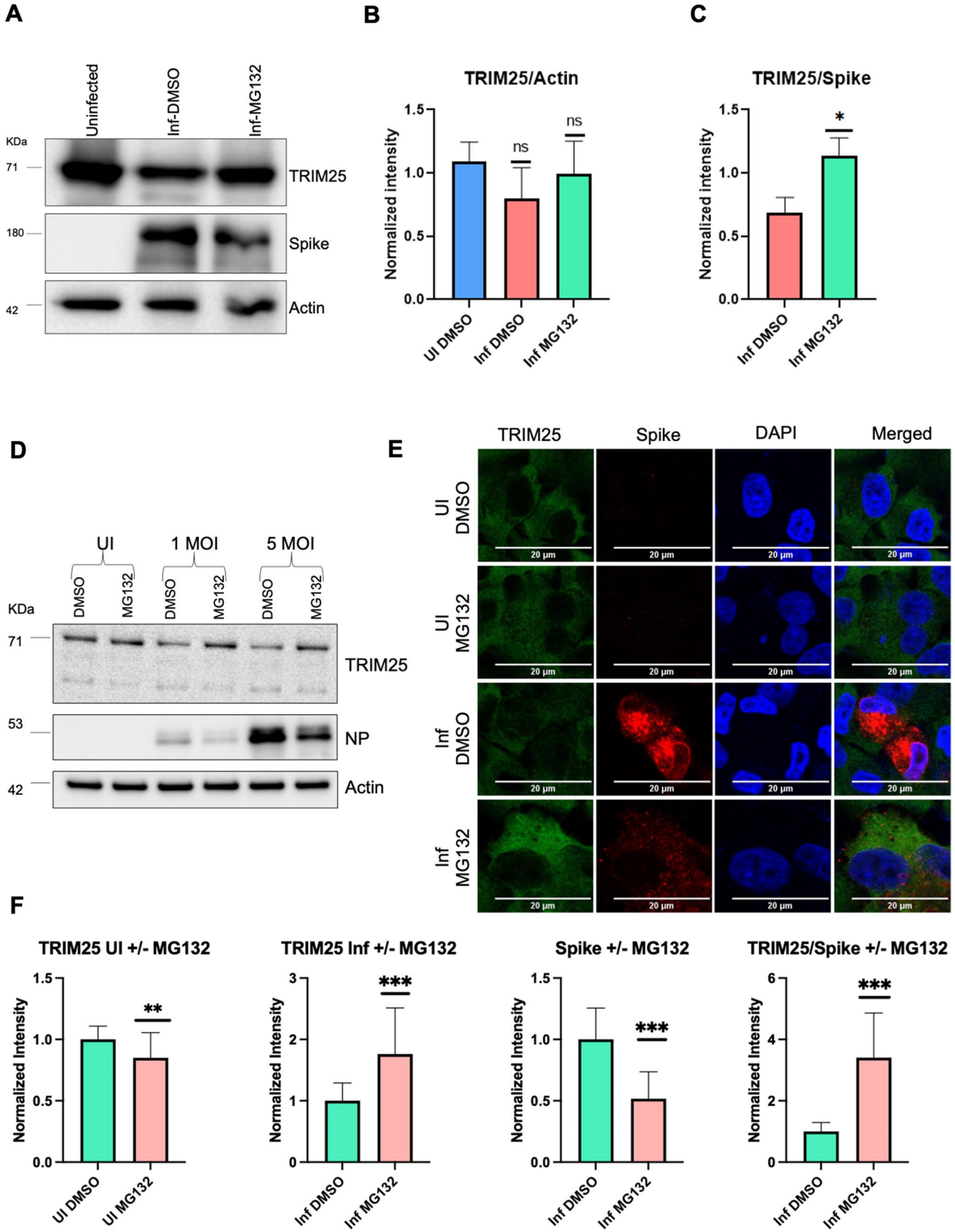
A
Uninfected
Inf-DMSO
Inf-MG132
KDa
71
180
42
TRIM25
Spike
Actin
B
TRIM25/Actin
Normalized intensity
1.5
1.0
0.5
0.0
ns
ns
UI DMSO
Inf DMSO
Inf MG132
C
TRIM25/Spike
Normalized intensity
1.5
1.0
0.5
0.0
*
Inf DMSO
Inf MG132
D
UI
1 MOI
5 MOI
DMSO
MG132
DMSO
MG132
DMSO
MG132
KDa
71
53
42
TRIM25
NP
Actin
E
TRIM25
Spike
DAPI
Merged
UI DMSO
UI MG132
Inf DMSO
Inf MG132
20 µm
F
TRIM25 UI +/- MG132
Normalized Intensity
1.5
1.0
0.5
0.0
**
UI DMSO
UI MG132
TRIM25 Inf +/- MG132
Normalized Intensity
3
2
1
0
***
Inf DMSO
Inf MG132
Spike +/- MG132
Normalized Intensity
1.5
1.0
0.5
0.0
***
Inf DMSO
Inf MG132
TRIM25/Spike +/- MG132
Normalized Intensity
6
4
2
0
***
Inf DMSO
Inf MG132

◂**Fig. 7** SARS-CoV-2 targets TRIM25 for proteasomal during infection. **A** Western blot analysis with cell lysates from HEK-ACE2 cells infected with SARS-CoV-2 at 1 MOI. 6 h post-infection, cells were treated with MG132 (10 μM) for 18 h followed by harvesting the cell lysates. **B**, **C** Quantification of fluorescence intensity of TRIM25, actin, and Spike from WB (Fig. 6a). Intensity was measured from three biological replicates. **D** Western blot analysis with cell lysates from A549-ACE2 cells infected with SARS-CoV-2 at 1 MOI or 5 MOI. 6 h post-infection cells were treated with MG132 (10 μM) for 18 h followed by harvesting the cell lysates. **E** A549-ACE2 cells were infected with SARS-CoV-2 at 1 MOI. 6 h post-infection cells were treated with MG132 (10 μM) for another 18 h. Cells were fixed with 4% PFA and proceeded with IFA. **F** Quantification of fluorescence intensity of TRIM25, Spike from IFA images (**F**). Intensity was measured from at least 18 cells from two biological replicates. Intensity is normalized to DMSO control. Bar graphs represent data from three technical replicates. Statistical significance of the data is represented as $*P<0.05$; $**P<0.01$; $***P<0.001$; *ns* not significant. Error bars represent mean + standard error

C-terminal cytoplasmic tail of ORF6 has been reported to be essential for its IFN antagonism [11]. We tested the importance of the same in the inhibition of the RIG-I function. We found that the C-terminal region, especially residues 52–61 of ORF6, were crucial for restricting RIG-I-mediated IFN induction; however, the lack of the C-terminal domain did not affect the direct interaction of ORF6 with RIG-I. This suggested that possibly post-translational modifications of RIG-I, which is known to regulate its activity and stability, may be affected by ORF6. Upon sensing a viral PAMP, the RIG-I protein undergoes the K63-linked ubiquitination by E3 ligase TRIM25, which is essential for its activation and downstream signaling [15]. Additional E3 ligase, Riplet/RNF135, attaches the K63-linked polyubiquitin chain to the C-terminal region of RIG-I [42]. This step of RLR signaling

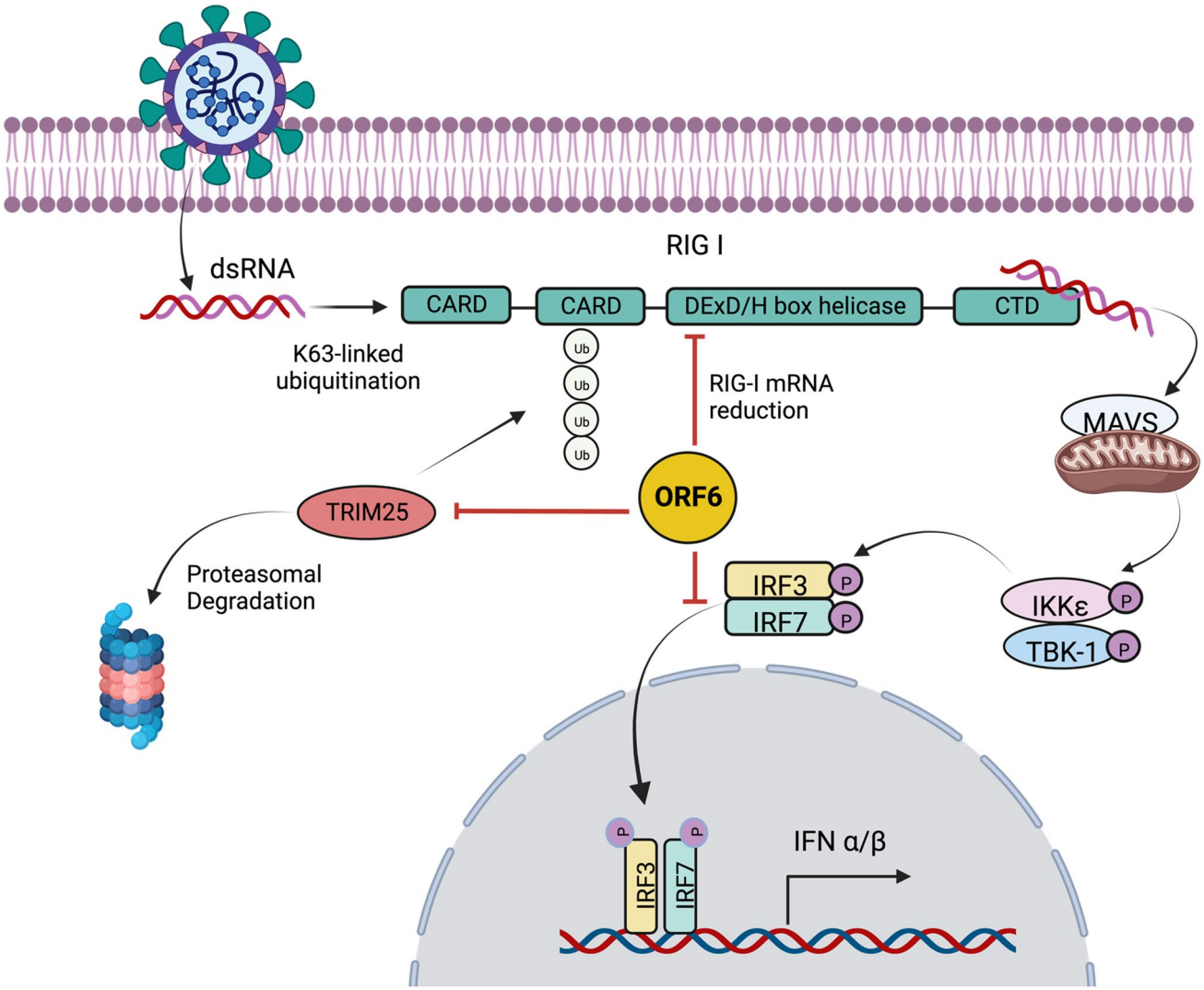

Fig. 8 Model of SARS-CoV-2 ORF6-mediated inhibition of K63-linked ubiquitination of RIG-I. Pictorial representation of stages of IFN induction pathway upon SARS-CoV-2 RNA recognition where TRIM25 mediates K63-linked ubiquitination of RIG-I CARD domain, which in turn gets activated and activates the downstream signaling pathway. In this study, we show that in addition to inhibiting nuclear translocation of IRF3, SARS-CoV-2 ORF6 targets TRIM25 for proteasomal degradation, which results in the reduced K63-linked ubiquitination of RIG-I and subsequent induction of type-I IFN

is often targeted by viral proteins, especially those of RNA viruses [43]. Our study showed that TRIM25-mediated K63-linked ubiquitination of RIG-I was significantly reduced in the presence of ORF6. However, the effect of ORF6 on other E3 ligase mediated K63-linked RIG-I ubiquitination is yet to be explored. This inhibitory effect was partially lost upon deletion of the C-terminal domain of ORF6, which explains the requirement of this region for type-I IFN antagonism. Further exploration of the effect of ORF6 on TRIM25 and RIG-I revealed that ORF6 targets TRIM25 for degradation. This phenotype is reversed partially by proteasome inhibitor as well as by deletion of the C-terminal domain of ORF6. Interestingly RIG-I expression was also reduced in the presence of ORF6, which was rescued upon deletion of either N- or C-terminal cytoplasmic tail. However, this reduction was not due to proteasomal targeting of RIG-I, as it could not be rescued by MG132 treatment. The degradation of TRIM25 was also observed in the case of SARS-CoV-2 infection, which was reversed upon treatment with a proteasomal inhibitor. MG132 treatment also led to reduced Spike protein production, which could be due to the restoration of TRIM25 and RIG-I-mediated antiviral response. Indeed, MG132 treatment during SARS-CoV-2 infection enhanced IFN and ISG mRNA expression (Supplementary Fig. 7), which confirms the co-option of proteasomal machinery by SARS-CoV-2 to antagonize type-I IFN induction. TRIM25-mediated ubiquitination of RIG-I has also been reported to be targeted by the NSP5 and nucleoprotein (N) of SARS-CoV-2[44, 45]. An additional layer of inhibition of the same by ORF6 highlights the significance of RIG-I signaling during SARS-CoV-2 infection.

Based on the collective results obtained in our study, we have proposed a working model for SARS-CoV-2 ORF6-mediated inhibition of type-I IFN induction, shown in Fig. 8. Previous studies have reported tight regulation of TRIM25 stability and its interaction with RIG-I to keep immune signaling pathway under check. RBR E3 ligase domains of HOIL-1L and HOIP proteins of the linear ubiquitin assembly complex (LUBAC) bind and target TRIM25 for proteasomal degradation [46]. How ORF6 targets TRIM25 for degradation remains to be investigated in detail and can potentially present an avenue for therapeutic intervention against SARS-CoV-2. The SARS-CoV-2 ORF6 protein is relatively conserved; however, few natural amino acid substitution and deletions have been observed in this protein [32, 47] and it will be interesting to examine the role of the same on the IFN-antagonism function of ORF6 [48]. One such example is D61L polymorphism that recently emerged in Omicron BA.2 and BA.4 and this loss-of-function mutation is demonstrated to exhibit reduced binding with Nup98, thus impairing the innate immune evasion [48]. Finally, ORF6 and other IFN antagonists of SARS-CoV-2, which may be dispensable for viral replication, can be removed from the viral genome to engineer attenuated strains, potentially useful as vaccines.

Supplementary Information The online version contains supplementary material available at https://doi.org/10.1007/s00018-023-05011-3.

Acknowledgements We are grateful to Prof. Adolfo Garcia Sastre, Microbiology Department, Icahn School of Medicine, New York, and Prof. Nevan J. Krogan, Cellular Molecular Pharmacology, University of California, San Francisco, for providing plasmids for studying IFN response and SARS-CoV-2 protein expression, respectively. We thank Rajesh Thangavel Yadav for his help with creating the 3D structure model of ORF6.

Author contributions Conceptualization, funding acquisition, project administration, supervision, resources: ST. Methodology, data curation, formal analysis, validation, visualization: OK, MS, RN, ST. Manuscript writing—review and editing: OK, MS, RN, ST.

Funding We acknowledge research funding to ST Lab and infrastructure support to IISc from the DBT-IISc partnership, DBT-BIRAC, Crypto Relief Fund, L & T Trust, and DST-FIST program to IISc.

Data availability All primary data associated with this study have been included in the manuscript. Any additional information query can be directed to corresponding author.

Declarations

Conflict of interest Authors have no competing interest to declare.

Ethical approval and consent to participate This study was conducted in compliance with institutional biosafety guidelines, (IBSC/IISc/ST/17/2020; IBSC/IISc/ST/18/2021). All experiments involving SARS-CoV-2 virus were performed in Viral BSL3 facility, following the Indian Council of Medical Research and Department of Biotechnology recommendations.

Consent for publication All the authors have provided consent for publication.

References

1. Coronaviridae Study Group of the International Committee on Taxonomy of V (2020) The species Severe acute respiratory syndrome-related coronavirus: classifying 2019-nCoV and naming it SARS-CoV-2. Nat Microbiol 5:536–544. https://doi.org/10.1038/s41564-020-0695-z
2. Finkel Y, Mizrahi O, Nachshon A, Weingarten-Gabbay S, Morgenstern D, Yahalom-Ronen Y et al (2021) The coding capacity of SARS-CoV-2. Nature 589:125–130. https://doi.org/10.1038/s41586-020-2739-1
3. Li JY, Zhou ZJ, Wang Q, He QN, Zhao MY, Qiu Y et al (2021) Innate immunity evasion strategies of highly pathogenic

coronaviruses: SARS-CoV, MERS-CoV, and SARS-CoV-2. Front Microbiol 12:770656. https://doi.org/10.3389/fmicb.2021.770656
4. Thorne LG, Reuschl AK, Zuliani-Alvarez L, Whelan MVX, Turner J, Noursadeghi M et al (2021) SARS-CoV-2 sensing by RIG-I and MDA5 links epithelial infection to macrophage inflammation. EMBO J 40:e107826. https://doi.org/10.15252/embj.2021107826
5. Yin X, Riva L, Pu Y, Martin-Sancho L, Kanamune J, Yamamoto Y et al (2021) MDA5 governs the innate immune response to SARS-CoV-2 in lung epithelial cells. Cell Rep 34:108628. https://doi.org/10.1016/j.celrep.2020.108628
6. Kouwaki T, Nishimura T, Wang G, Oshiumi H (2021) RIG-I-Like receptor-mediated recognition of viral genomic RNA of severe acute respiratory syndrome coronavirus-2 and viral escape from the host innate immune responses. Front Immunol 12:700926. https://doi.org/10.3389/fimmu.2021.700926
7. Hiscott J, Nguyen TL, Arguello M, Nakhaei P, Paz S (2006) Manipulation of the nuclear factor-kappaB pathway and the innate immune response by viruses. Oncogene 25:6844–6867. https://doi.org/10.1038/sj.onc.1209941
8. Platanias LC (2005) Mechanisms of type-I- and type-II-interferon-mediated signalling. Nat Rev Immunol 5:375–386. https://doi.org/10.1038/nri1604
9. Darnell JE Jr, Kerr IM, Stark GR (1994) Jak-STAT pathways and transcriptional activation in response to IFNs and other extracellular signaling proteins. Science 264:1415–1421. https://doi.org/10.1126/science.8197455
10. Garcia-Sastre A (2017) Ten strategies of interferon evasion by viruses. Cell Host Microbe 22:176–184. https://doi.org/10.1016/j.chom.2017.07.012
11. Lei X, Dong X, Ma R, Wang W, Xiao X, Tian Z et al (2020) Activation and evasion of type I interferon responses by SARS-CoV-2. Nat Commun 11:3810. https://doi.org/10.1038/s41467-020-17665-9
12. Xia H, Cao Z, Xie X, Zhang X, Chen JY, Wang H et al (2020) Evasion of type I interferon by SARS-CoV-2. Cell Rep 33:108234. https://doi.org/10.1016/j.celrep.2020.108234
13. V'Kovski P, Kratzel A, Steiner S, Stalder H, Thiel V (2021) Coronavirus biology and replication: implications for SARS-CoV-2. Nat Rev Microbiol 19:155–170. https://doi.org/10.1038/s41579-020-00468-6
14. Wu A, Peng Y, Huang B, Ding X, Wang X, Niu P et al (2020) Genome composition and divergence of the novel coronavirus (2019-nCoV) Originating in China. Cell Host Microbe 27:325–328. https://doi.org/10.1016/j.chom.2020.02.001
15. Gack MU, Shin YC, Joo CH, Urano T, Liang C, Sun L et al (2007) TRIM25 RING-finger E3 ubiquitin ligase is essential for RIG-I-mediated antiviral activity. Nature 446:916–920. https://doi.org/10.1038/nature05732
16. Gordon DE, Jang GM, Bouhaddou M, Xu J, Obernier K, White KM et al (2020) A SARS-CoV-2 protein interaction map reveals targets for drug repurposing. Nature 583:459–468. https://doi.org/10.1038/s41586-020-2286-9
17. Versteeg GA, Rajsbaum R, Sanchez-Aparicio MT, Maestre AM, Valdiviezo J, Shi M et al (2013) The E3-ligase TRIM family of proteins regulates signaling pathways triggered by innate immune pattern-recognition receptors. Immunity 38:384–398. https://doi.org/10.1016/j.immuni.2012.11.013
18. Edelheit O, Hanukoglu A, Hanukoglu I (2009) Simple and efficient site-directed mutagenesis using two single-primer reactions in parallel to generate mutants for protein structure-function studies. BMC Biotechnol 9:61. https://doi.org/10.1186/1472-6750-9-61
19. Case JB, Bailey AL, Kim AS, Chen RE, Diamond MS (2020) Growth, detection, quantification, and inactivation of SARS-CoV-2. Virology 548:39–48. https://doi.org/10.1016/j.virol.2020.05.015
20. Liu G, Lee JH, Parker ZM, Acharya D, Chiang JJ, van Gent M et al (2021) ISG15-dependent activation of the sensor MDA5 is antagonized by the SARS-CoV-2 papain-like protease to evade host innate immunity. Nat Microbiol 6:467–478. https://doi.org/10.1038/s41564-021-00884-1
21. Moustaqil M, Ollivier E, Chiu HP, Van Tol S, Rudolffi-Soto P, Stevens C et al (2021) SARS-CoV-2 proteases PLpro and 3CLpro cleave IRF3 and critical modulators of inflammatory pathways (NLRP12 and TAB1): implications for disease presentation across species. Emerg Microbes Infect 10:178–195. https://doi.org/10.1080/22221751.2020.1870414
22. Fu YZ, Wang SY, Zheng ZQ, Yi H, Li WW, Xu ZS et al (2021) SARS-CoV-2 membrane glycoprotein M antagonizes the MAVS-mediated innate antiviral response. Cell Mol Immunol 18:613–620. https://doi.org/10.1038/s41423-020-00571-x
23. Hayn M, Hirschenberger M, Koepke L, Nchioua R, Straub JH, Klute S et al (2021) Systematic functional analysis of SARS-CoV-2 proteins uncovers viral innate immune antagonists and remaining vulnerabilities. Cell Rep 35:109126. https://doi.org/10.1016/j.celrep.2021.109126
24. Li JY, Liao CH, Wang Q, Tan YJ, Luo R, Qiu Y et al (2020) The ORF6, ORF8 and nucleocapsid proteins of SARS-CoV-2 inhibit type I interferon signaling pathway. Virus Res 286:198074. https://doi.org/10.1016/j.virusres.2020.198074
25. Shemesh M, Aktepe TE, Deerain JM, McAuley JL, Audsley MD, David CT et al (2021) Correction: SARS-CoV-2 suppresses IFN-beta production mediated by NSP1, 5, 6, 15, ORF6 and ORF7b but does not suppress the effects of added interferon. PLoS Pathog 17:e1010146. https://doi.org/10.1371/journal.ppat.1010146
26. Stukalov A, Girault V, Grass V, Karayel O, Bergant V, Urban C et al (2021) Multilevel proteomics reveals host perturbations by SARS-CoV-2 and SARS-CoV. Nature 594:246–252. https://doi.org/10.1038/s41586-021-03493-4
27. Yuen CK, Lam JY, Wong WM, Mak LF, Wang X, Chu H et al (2020) SARS-CoV-2 nsp13, nsp14, nsp15 and orf6 function as potent interferon antagonists. Emerg Microbes Infect 9:1418–1428. https://doi.org/10.1080/22221751.2020.1780953
28. Zhang Q, Chen Z, Huang C, Sun J, Xue M, Feng T et al (2021) Severe Acute respiratory syndrome coronavirus 2 (SARS-CoV-2) Membrane (M) and Spike (S) proteins antagonize host type I interferon response. Front Cell Infect Microbiol 11:766922. https://doi.org/10.3389/fcimb.2021.766922
29. Vazquez C, Swanson SE, Negatu SG, Dittmar M, Miller J, Ramage HR et al (2021) SARS-CoV-2 viral proteins NSP1 and NSP13 inhibit interferon activation through distinct mechanisms. PLoS ONE 16:e0253089. https://doi.org/10.1371/journal.pone.0253089
30. Chan JF, Kok KH, Zhu Z, Chu H, To KK, Yuan S et al (2020) Genomic characterization of the 2019 novel human-pathogenic coronavirus isolated from a patient with atypical pneumonia after visiting Wuhan. Emerg Microbes Infect 9:221–236. https://doi.org/10.1080/22221751.2020.1719902
31. Frieman M, Yount B, Heise M, Kopecky-Bromberg SA, Palese P, Baric RS (2007) Severe acute respiratory syndrome coronavirus ORF6 antagonizes STAT1 function by sequestering nuclear import factors on the rough endoplasmic reticulum/Golgi membrane. J Virol 81:9812–9824. https://doi.org/10.1128/JVI.01012-07

32. Riojas MA, Frank AM, Puthuveetil NP, Flores B, Parker M, King SP et al (2020) A rare deletion in SARS-CoV-2 ORF6 dramatically alters the predicted three-dimensional structure of the resultant protein. bioRxiv. https://doi.org/10.1101/2020.06.09.134460
33. Rehwinkel J, Gack MU (2020) RIG-I-like receptors: their regulation and roles in RNA sensing. Nat Rev Immunol 20:537–551. https://doi.org/10.1038/s41577-020-0288-3
34. Choi Y, Bowman JW, Jung JU (2018) Autophagy during viral infection - a double-edged sword. Nat Rev Microbiol 16:341–354. https://doi.org/10.1038/s41579-018-0003-6
35. Gao G, Luo H (2006) The ubiquitin-proteasome pathway in viral infections. Can J Physiol Pharmacol 84:5–14. https://doi.org/10.1139/y05-144
36. Min YQ, Huang M, Sun X, Deng F, Wang H, Ning YJ (2021) Immune evasion of SARS-CoV-2 from interferon antiviral system. Comput Struct Biotechnol J 19:4217–4225. https://doi.org/10.1016/j.csbj.2021.07.023
37. Thoms M, Buschauer R, Ameismeier M, Koepke L, Denk T, Hirschenberger M et al (2020) Structural basis for translational shutdown and immune evasion by the Nsp1 protein of SARS-CoV-2. Science 369:1249–1255. https://doi.org/10.1126/science.abc8665
38. Guo G, Gao M, Gao X, Zhu B, Huang J, Luo K et al (2021) SARS-CoV-2 non-structural protein 13 (nsp13) hijacks host deubiquitinase USP13 and counteracts host antiviral immune response. Signal Transduct Target Ther 6:119. https://doi.org/10.1038/s41392-021-00509-3
39. Hsu JC, Laurent-Rolle M, Pawlak JB, Wilen CB, Cresswell P (2021) Translational shutdown and evasion of the innate immune response by SARS-CoV-2 NSP14 protein. Proc Natl Acad Sci U S A. https://doi.org/10.1073/pnas.2101161118
40. Miorin L, Kehrer T, Sanchez-Aparicio MT, Zhang K, Cohen P, Patel RS et al (2020) SARS-CoV-2 Orf6 hijacks Nup98 to block STAT nuclear import and antagonize interferon signaling. Proc Natl Acad Sci USA 117:28344–28354. https://doi.org/10.1073/pnas.2016650117
41. Addetia A, Lieberman NAP, Phung Q, Hsiang TY, Xie H, Roychoudhury P et al (2021) SARS-CoV-2 ORF6 Disrupts Bidirectional Nucleocytoplasmic Transport through Interactions with Rae1 and Nup98. mBio. https://doi.org/10.1128/mBio.00065-21
42. Riplet/RNF135, a RING finger protein, ubiquitinates RIG-I to promote interferon-beta induction during the early phase of viral infection
43. Liu Y, Olagnier D, Lin R (2016) Host and viral modulation of RIG-I-mediated antiviral immunity. Front Immunol 7:662. https://doi.org/10.3389/fimmu.2016.00662
44. Wu Y, Ma L, Zhuang Z, Cai S, Zhao Z, Zhou L et al (2020) Main protease of SARS-CoV-2 serves as a bifunctional molecule in restricting type I interferon antiviral signaling. Signal Transduct Target Ther 5:221. https://doi.org/10.1038/s41392-020-00332-2
45. Zhao Y, Sui L, Wu P, Wang W, Wang Z, Yu Y et al (2021) A dual-role of SARS-CoV-2 nucleocapsid protein in regulating innate immune response. Signal Transduct Target Ther 6:331. https://doi.org/10.1038/s41392-021-00742-w
46. Inn KS, Gack MU, Tokunaga F, Shi M, Wong LY, Iwai K et al (2011) Linear ubiquitin assembly complex negatively regulates RIG-I- and TRIM25-mediated type I interferon induction. Mol Cell 41:354–365. https://doi.org/10.1016/j.molcel.2010.12.029
47. Queromes G, Destras G, Bal A, Regue H, Burfin G, Brun S et al (2021) Characterization of SARS-CoV-2 ORF6 deletion variants detected in a nosocomial cluster during routine genomic surveillance, Lyon, France. Emerg Microbes Infect 10:167–177. https://doi.org/10.1080/22221751.2021.1872351
48. Kehrer T, Cupic A, Ye C, Yildiz S, Bouhhadou M, Crossland NA et al (2022) Impact of SARS-CoV-2 ORF6 and its variant polymorphisms on host responses and viral pathogenesis. bioRxiv. https://doi.org/10.1101/2022.10.18.512708